

Multi-messenger constraints on Abelian-Higgs cosmic string networks

Mark Hindmarsh^{a,b} and Jun'ya Kume^{c,d}

^aDepartment of Physics and Helsinki Institute of Physics, PL 64, FI-00014 University of Helsinki, Finland

^bDepartment of Physics and Astronomy, University of Sussex, Falmer, Brighton BN1 9QH, U.K.

^cResearch Center for the Early Universe (RESCEU), Graduate School of Science, The University of Tokyo, Hongo 7-3-1 Bunkyo-ku, Tokyo 113-0033, Japan

^dDepartment of Physics, Graduate School of Science, The University of Tokyo, Hongo 7-3-1 Bunkyo-ku, Tokyo 113-0033, Japan

E-mail: mark.hindmarsh@helsinki.fi, kjun0107@resceu.s.u-tokyo.ac.jp

Abstract. Nielsen-Olesen vortices in the Abelian-Higgs (AH) model are the simplest realisations of cosmic strings in a gauge field theory. Large-scale numerical solutions show that the dominant decay channel of a network of AH strings produced from random initial conditions is classical field radiation. However, they also show that with special initial conditions, loops of string can be created for which classical field radiation is suppressed, and which behave like Nambu-Goto (NG) strings with a dominant decay channel into gravitational radiation. This indicates that cosmic strings are generically sources of both high-energy particles and gravitational waves. Here we adopt a simple parametrisation of the AH string network allowing for both particle and gravitational wave production, which sets the basis for a “multi-messenger” investigation of this model. We find that, in order to explain the NANOGrav detection of a possible gravitational wave background, while satisfying the constraint on NG-like loop production from simulations and bounds from the cosmic microwave background, the tension of the AH string in Planck units $G\mu$ and the fraction of the NG-like loops f_{NG} should satisfy $G\mu f_{\text{NG}}^{2.6} \gtrsim 3.2 \times 10^{-13}$ at 95% confidence. On the other hand, for such string tensions, constraints from the diffuse gamma-ray background (DGRB) indicate that more than 97% of the total network energy should be converted to dark matter (DM) or dark radiation. We also consider joint constraints on the annihilation cross-section, the mass, and the relic abundance of DM produced by decays of strings. For example, for a DM mass of 500 GeV, the observed relic abundance can be explained by decaying AH strings that also account for the NANOGrav signal.

Contents

1	Introduction	1
2	Multi-messenger signals from the Abelian-Higgs string network	3
2.1	Particle emission from the strings	3
2.2	Gravitational wave background from Nambu-Goto-like loops	4
3	Multi-messenger measurements and its constraint on the AH string	7
3.1	Big-Bang nucleosynthesis and gamma-ray constraints	7
3.2	Mapping the NANOGrav 12.5yr result	9
3.3	Combined constraints and implications for the AH model	12
4	Discussion	15

1 Introduction

Cosmic strings are linear concentrations of energy with a cosmological size that may have been produced at early-universe phase transitions in a variety of high-energy physics scenarios [1–4]. In the traditional picture of cosmic strings, they are treated as infinitely thin line-like objects. Then the strings are expected to evolve according to the Nambu-Goto (NG) equation [5–7] and additional re-connection rule when strings cross each other [8–10]. Within this picture, an observable stochastic gravitational wave background (SGWB) can be generated by the slowly-decaying loops of cosmic string [11]. The most stringent constraints were provided by the non-observation of such a SGWB with the Pulsar Timing Array (PTA) experiments [12–14], which gives $G\mu \lesssim 10^{-10}$ (with μ the string tension and G Newton’s constant) for the pure NG-loops [15, 16]. Recently, however, PTA experiments have reported the evidence of the common stochastic process in their latest results [17–20]. Although the evidence for spatial correlations, which is indispensable to declare the SGWB detection, is as yet negligible, it is intriguing to consider the possibility that these results are associated with cosmic string [21–25]¹.

In order for there to be stable string solutions, the Standard Model needs to be extended with extra spontaneously broken symmetry. The simplest way to extend the gauge symmetry of the Standard Model is with an extra U(1) symmetry, so that the new gauge field and associated scalar are described by the Abelian-Higgs (AH) model. This possesses string solutions [28], which have been well investigated both analytically and numerically. The evolution of the AH string network is tested by the large scale numerical simulation based on the underlying classical AH field theory [29–36], in which scaling behavior of the network was observed, meaning that the mean inter-string distance grows in proportion to time. Strings in extensions with non-Abelian symmetries behave in a similar way [37].

While the observation of the scaling agrees with the modelling based on the NG approximation, AH simulations show that loops of string decay as fast as causally allowed through the production of classical scalar and gauge radiation [38, 39]. On the basis of this fast decay, Ref. [40] put bounds on the string tension from the light element abundances and the Diffuse

¹See also recent studies which analyze PPTA DR2 with modeled common red noise and gives the upper bound on the string tension [26, 27]

Gamma-Ray background (DGRB), which might be affected by a chain of decay products in the visible sector from the AH strings. If the decay products include dark matter (DM), further constraints follow from the dark matter relic density [41]. In a recent simulation of the AH string loops [39, 42], however, it was shown that field configurations whose evolution is well approximated by NG dynamics can be created by special initial conditions. Such NG-like strings, if large enough, would decay primarily through gravitational waves. Although NG-like strings have not been observed in AH network simulations, the simulations can only put an upper bound on the fraction of such loops. Therefore we must allow for the emission of both high energy particles from the network and gravitational waves.

This dual emission possibility motivates the investigation of possible multi-messenger signals from the AH string in this study. Following the previous work [40], we first characterize the energy injection to the visible sector from the AH string network. As pointed out in Ref. [43], the string field can generically couple to the Standard Model (SM) Higgs via the portal coupling. Therefore, a significant fraction of the network energy might end up in the SM particles, which could affect the consequence of the Big-Bang nucleosynthesis (BBN) and the DGRB measurement. This would also be the case for models in which the gauge symmetry of the AH model is an anomaly-free U(1) of the Standard Model such as $B - L$, where B is baryon number and L lepton number, such as might be expected in Grand Unified Theories [44, 45]. Assuming that AH strings dominantly decay into SM Higgs, the authors of Ref. [40] translated BBN constraints on the decaying massive particles and the upper bound on the cascade energy density into the bounds on the string tension of the AH model, which depends on this energy fraction. Here we update these bounds by applying the latest results on the BBN constraint [46] and the cascade energy density [47]. We also briefly discuss constraint on DM production based on Ref. [41], in which the energy injection is characterized in the same way.

The intensity of the SGWB from NG-like loops in the AH model is uncertain. The authors of Ref. [42] identified the critical length scale in their simulation above which loops are well approximated by the NG equation, and gravitational radiation presumably becomes dominant. The initial condition of the loop configurations used there, however, were somewhat special. In Ref. [39], the AH loops were created from random initial conditions appropriate for cosmological network simulations [48]. Long-lived NG-like loops were not observed in a sample of over 30 large loops, and the fraction of such loops was bounded at around 10%. Following this study, we parameterize this fraction as f_{NG} to estimate the possible SGWB in the AH model. To compare it with the NANOGrav 12.5yr result [17], which assumed the power-law spectrum of the SGWB, we introduce a likelihood model and construct a mapping from the power-law parameters to the AH string parameters.

The rest of the paper is organized as follows. In Sec. 2, we characterize the particle emission from the AH string network and the SGWB from NG-like loops by introducing two parameters in the model. Based on this characterization, we derive the constraints on the AH model from the optical observation and the SGWB observation in Sec. 3. We first apply the BBN constraints and the cascade energy upper bound to the decay products of the AH strings. Then we investigate the allowed parameter region of the AH model inferred from the NANOGrav 12.5yr result. By combining these two result, we derive constraints on the model parameters including the possibility of DM production from strings. Sec. 4 is devoted to the discussion.

2 Multi-messenger signals from the Abelian-Higgs string network

In the following, we study the AH model, whose Lagrangian density is given by

$$\mathcal{L} = g^{\mu\nu} D_\mu \phi D_\nu \phi^* + V(\phi) + \frac{1}{4e^2} g^{\mu\rho} g^{\nu\sigma} F_{\mu\nu} F_{\rho\sigma}, \quad (2.1)$$

where $g_{\mu\nu}$ is a metric, $\phi(x)$ is a complex scalar field with the potential $V(\phi) = \frac{1}{4}\lambda(|\phi|^2 - |\phi_0|^2)$, $A_\mu(x)$ is a vector field and $D_\mu = \partial_\mu - iA_\mu$ is the covariant derivative. Throughout this work, the critical coupling $\beta \equiv \lambda/2e^2 = 1$ is assumed for simplicity, where the string tension is given by $\mu = 2\pi\phi_0^2$. We first make a brief review of the characterization of the particle radiation from the cosmic string network based on Ref. [40]. Then we characterize the gravitational wave background from Nambu-Goto-like loops by utilizing the parameter advocated in Ref. [39].

2.1 Particle emission from the strings

Numerical simulations of the Abelian-Higgs (AH) string networks based on the classical field theory show that loops of string quickly decay into classical radiation of the scalar and gauge field of the theory. Since the string scalar field generically couples to the SM Higgs doublet Φ through a portal coupling, for example $\lambda_p|\phi|^2|\Phi|^2$ [43], the radiation is expected to end up in the SM particles. This also happens if the gauge field couples to the SM through, for example, mixing with hypercharge or $B - L$.

Following the notation in Ref. [40], we parametrise the fraction of the energy which is released from the string network and results in the form of SM particles as β_{SM}^2 . Considering covariant energy conservation, the total power per unit volume injected into the SM plasma becomes

$$Q_h = -\beta_{\text{SM}}^2 [\dot{\rho}_s + 3H(1+w_s)\rho_s], \quad (2.2)$$

where ρ_s is the total energy density of the strings, w_s is their average equation of state parameter and H is the Hubble parameter. Assuming that ρ_s accounts for a subdominant fraction of the total energy density of the universe ρ , Q_h can be approximated as

$$\frac{Q_h}{H\rho} \simeq 3\beta_{\text{SM}}^2(w - w_s)\Omega_s, \quad (2.3)$$

where w is the total equation of state parameter and $\Omega_s \equiv \rho_s/\rho$. As a result, the injected energy density in the visible sector is estimated as

$$\Delta\rho_h(t) \simeq Q_h t \simeq 3\beta_{\text{SM}}^2(w - w_s)\rho_s/\alpha^2, \quad (2.4)$$

with $\alpha = \sqrt{2}$ for the radiation dominated era and $\alpha = \sqrt{3/2}$ for the matter dominated era. In order to connect with the result of numerical simulation, let us introduce following parameters

$$x \equiv \alpha\sqrt{\mu/\rho_s t^2}, \quad (2.5)$$

$$\bar{\gamma}_{\text{SM}} \equiv 3\beta_{\text{SM}}^2(w - w_s)/x^2, \quad (2.6)$$

which allow us to rewrite $\Delta\rho_h$ in a simplified form

$$\Delta\rho_h(t) = \bar{\gamma}_{\text{SM}} \frac{\mu}{t^2}. \quad (2.7)$$

From the field theoretical simulation of AH model performed in Refs. [31, 38], these parameters are evaluated as $x \simeq 0.7$ and $w_s = -0.13$ for the radiation era, $x \simeq 0.9$ and $w_s = -0.15$ for the matter era respectively. Combining these values, we obtain

$$\bar{\gamma}_{\text{SM}} \simeq \begin{cases} 2.8\beta_{\text{SM}}^2 & (\text{RD era}) \\ 0.5\beta_{\text{SM}}^2 & (\text{MD era}). \end{cases} \quad (2.8)$$

In the following, we assume that this fraction of the classical radiation β_{SM}^2 dominantly decays into the SM Higgs (and thus we denote the energy injection as $\Delta\rho_h$). Note that the information of the coupling constant and the dynamical evolution of the particles is implicitly encoded in β_{SM} . We do not assume a specific coupling in this work and so perform a model-independent analysis by virtue of this characterization.

This parametrisation is also applicable to the calculation of DM relic abundance as investigated in Ref. [41]. We will come back to this point in the last part of Sec. 3.3.

2.2 Gravitational wave background from Nambu-Goto-like loops

Assuming the Nambu-Goto (NG) dynamics of the strings, the SGWB from the cosmic string network is dominantly generated by the oscillation of the sub-horizon loops. Therefore, the number density $n(l, t)$ of non-self-intersecting, sub-horizon cosmic string loops of invariant length l at cosmic time t is the necessary ingredient in the evaluation of the SGWB spectrum. As discussed in Ref. [11], there are two different NG-simulation based models, the BOS model [49, 50] and the LRS model [51, 52]. The most important consequence of LRS model is the dominance of small loops, which was not observed in the BOS simulation. The reasons for the difference is not fully clear. Here, in the absence of any information about the size distribution of NG-like loops in the AH simulations, we adopt the BOS model as a benchmark for the NG loop distribution, due to its greater simplicity.

In the BOS model [49], the number density for non-self-intersecting loops directly from NG simulations is characterized as

$$n_{r,r}(l, t) = \frac{0.18}{t^{3/2}(l + \Gamma G\mu t)^{5/2}} \Theta(0.1 - l/t), \quad (2.9)$$

$$n_{r,m}(l, t) = \frac{0.18(2H_0\sqrt{\Omega_r})^{3/2}(1+z)^3}{(l + \Gamma G\mu t)^{5/2}} \Theta(0.09t_{\text{eq}}/t - \Gamma G\mu - l/t), \quad (2.10)$$

$$n_{m,m}(l, t) = \frac{0.27 - 0.45(l/t)^{0.31}}{t^2(l + \Gamma G\mu t)^2} \Theta(0.18 - l/t), \quad (2.11)$$

where H_0 is the Hubble constant, Ω_r is the density parameter of the radiation, t_{eq} represents the cosmic time of radiation-matter equality and Γ is a constant which characterises the average total power emitted by a loop as $\Gamma G\mu^2$. Here the subscript “r,m”, for example, represents the loops produced in the radiation era and emitting GWs in matter era. Note that Eq. (2.10) matches to Eq. (2.9) in the early radiation era. With this number density $n(l, t)$, the present day spectrum of the SGWB can be calculated from

$$\Omega_{\text{gw}}^{(\text{NG})}(f) \equiv \frac{1}{\rho_c} \frac{d \ln \rho_{\text{gw}}^{(\text{NG})}}{d \ln f} = \frac{8\pi f G^2 \mu^2}{3H_0^2} \sum_{n=1}^{\infty} C_n(f) P_n, \quad (2.12)$$

where

$$C_n(f) = \frac{2n}{f^2} \int_0^{\infty} \frac{dz}{H(z)(1+z)^6} n\left(\frac{2n}{(1+z)f}, t(z)\right) \quad (2.13)$$

with $H(z)$ and $t(z)$ being the Hubble parameter and cosmic time at redshift z . The function $C_n(f)$ indicates the number density of loops emitting GWs observed at frequency f in the n -th harmonic, while P_n is the average GW power emitted by the n -th harmonic of a loop. The sum satisfies

$$\sum_{n=1}^{\infty} P_n = \Gamma. \quad (2.14)$$

The constants P_n depend on the average shape of the loops and hereafter we adopt the “smoothed” model constructed from the numerical simulation taking into account the gravitational backreaction [50] and take $\Gamma = 50$, which is also indicated by the simulations.

While the large-scale field theory simulations in the Abelian-Higgs model indicate that a loop of length L decays into massive radiation in a time less than $0.25L$, simulations of individual loops in the Abelian-Higgs model shows that NG-like string can be generated with carefully chosen initial conditions [39, 42]. This result motivates us to consider the possibility that a certain fraction of the loops obeys NG dynamics in the AH network. Here we parameterise this uncertainty by allowing a fraction f_{NG} of loops to survive to radiate only gravitationally [39]. As a first approximation, we model the distribution of NG-like loops in the AH network as $f_{\text{NG}}(l, t)$ and thus the SGWB as

$$\Omega_{\text{gw}}^{(\text{AH})}(f) = f_{\text{NG}} \Omega_{\text{gw}}^{(\text{NG})}(f). \quad (2.15)$$

Since NG-like long-lived loops were not observed in an ensemble of randomly generated AH loops, the upper bound is estimated as $f_{\text{NG}} \lesssim 0.1$ [39].

We should note that use of the loop number density Eq. (2.9)–(2.11) is only a first approximation. This number density is based on the NG string simulation where the scaling of the infinite strings is maintained solely by the loop production at the intersection. On the other hand, scaling in AH model is also assisted by classical radiation. We therefore might expect the NG-like loops to be produced with a different initial size. The shapes of the NG-like loops in an AH network may also be different, as the formation process is accompanied by a burst of classical radiation as the loop collapses and finds its stable configuration. This could lead to a different gravitational wave power parameter Γ . We also neglect a next-order effect, due to particle emission at cusps and kinks, which reduces the lifetimes of smaller loops [42, 53]. This modifies the GW spectrum as investigated in Ref. [54]. For the BOS model, however, the effect of particle emission is to impose a high frequency cutoff,² well above the nanohertz range of frequencies we consider. We will leave the development of improved models to future work, with the expectation that the correction in Eq. (2.15) is $\mathcal{O}(1)$ ³.

In evaluating the gravitational wave power spectrum Eq. (2.15), we assume a Λ CDM cosmology for which

$$H(z) = H_0 \sqrt{\Omega_{\Lambda} + (1+z)^3 \Omega_m + G(z)(1+z)^4 \Omega_r}, \quad (2.16)$$

and take Planck 2018 fiducial parameters [57] $\Omega_m = 0.308$, $\Omega_r = 9.1476 \times 10^{-5}$, $\Omega_{\Lambda} = 1 - \Omega_m - \Omega_r$ and $H_0 = 67.8$ km/s/Mpc, as adopted in Ref. [11]. The change of the relativistic

²See also Ref. [55] which studies the effect of the particle radiation for the LRS model [51].

³For example, assuming that the loop size at the production well agrees with the BOS model, the authors of Ref. [56] quantify the effect of classical radiation on the efficiency of loop production in the string network based on Ref. [34], which results in the suppression of the overall amplitude of SGWB only by a factor ~ 2 .

degrees of freedom is encoded in

$$\mathcal{G}(z) = \frac{g_*(z)g_s^{4/3}(0)}{g_*(0)g_s^{4/3}(z)}, \quad (2.17)$$

where $g_*(z)$ and $g_s(z)$ are the effective number of relativistic and entropic degrees of freedom. To estimate it with SM particle contents, we use $g_*(T)$ and $g_s(T)$ tabulated in the micrOMEGAs [58], based on the calculation in Ref. [59]. Note that the models of loop number density (2.9)–(2.11) do not take into account the variation in $\mathcal{G}(z)$. Assuming that the dominant loops at any given time are relics of the earlier times, this effect was approximately taken into account in Ref. [50] as follows⁴. If $\mathcal{G}(z)$ is constant for a while in the RD era, $\mathcal{G}(z) = \mathcal{G}$, the expansion rate and the cosmic time becomes

$$H(z) = (1+z)^2 H_0 \sqrt{\Omega_r \mathcal{G}}, \quad (2.18)$$

$$t(z) = \frac{1}{2(1+z)^2 H_0 \sqrt{\Omega_r \mathcal{G}}}, \quad (2.19)$$

which results in the loop number density

$$n_{r,r}(l, t) = \frac{0.18 \{2H_0 \sqrt{\Omega_r \mathcal{G}}\}^{3/2} (1+z)^3}{(l + \Gamma G \mu t)^{5/2}} \Theta(0.1 - l/t). \quad (2.20)$$

Once loops of a certain size are no longer produced in significant numbers, their number density merely dilutes as $(1+z)^3$, and the loops shrink due to the gravitational wave emission. Both these effects, taken into account in Eq. (2.20), are responsible for the late time behavior of the loops and \mathcal{G} should be identified as the value at their production time. Since in the BOS model the loop production is highly peaked at $l/t \sim 0.1$, the typical time when the loop with length l at time t was produced is given as

$$t_l = 10(l + \Gamma \mu t). \quad (2.21)$$

With this expression, the z dependence of \mathcal{G} can be recovered as

$$n_{r,r}(l, t) \simeq \frac{0.18 \{2H_0 \sqrt{\Omega_r \mathcal{G}(z(t_l))}\}^{3/2} (1+z)^3}{(l + \Gamma G \mu t)^{5/2}} \Theta(0.1 - l/t). \quad (2.22)$$

Precisely speaking, this approximation is valid when $\mathcal{G}(z(t_1))$ is constant and one needs to take into account its variation for a smoother dependence of Ω_{gw} on f . However, for most values of $G\mu$ of our interest, the SGWB within PTA frequency range is dominated by the loops surviving from the radiation era (2.10) and this subtlety does not affect our result.

In Fig. 1, we plot the spectrum of SGWB (2.15) with the benchmark parameters $(G\mu, f_{\text{NG}}) = (10^{-10}, 1)$, $(10^{-8}, 0.1)$, and $(10^{-7}, 0.05)$. We also plot the previously obtained upper bounds by PTA experiments [12–14], which is comparable to the amplitude of SGWB estimated from the recently reported common stochastic process [17–20]. The fraction of NG-like loops $f_{\text{NG}} = 0.1$, which is assumed for the purple line, is the highest allowed value in our model. On the other hand, $G\mu = 10^{-7}$ is the highest string tension which satisfies the

⁴The effect of the variation in the degrees of freedom is analytically discussed in Ref. [60].

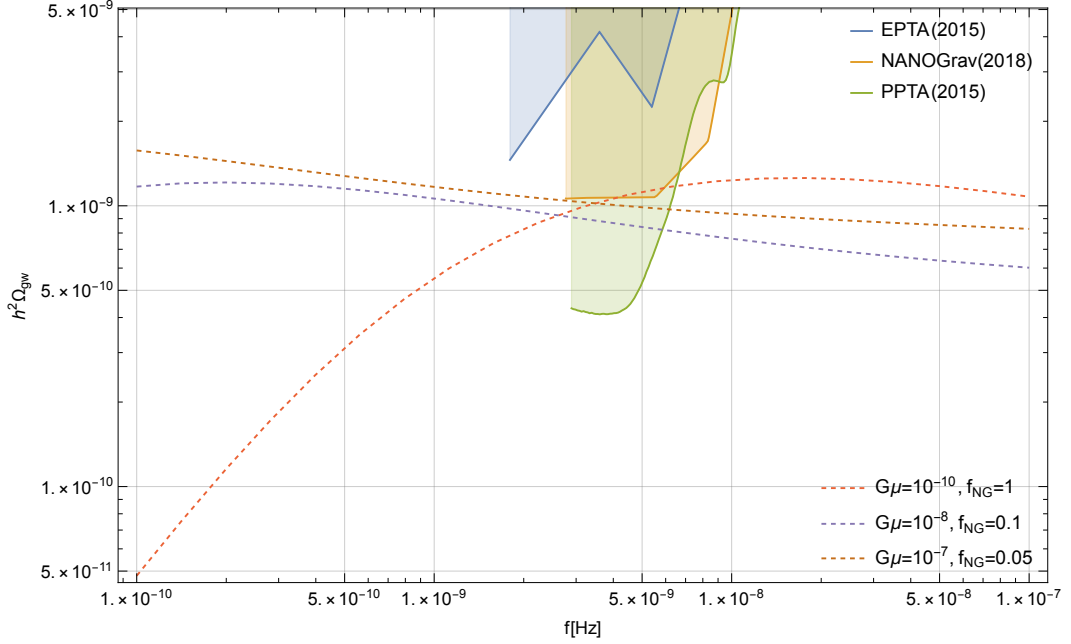


Figure 1. Examples of GWB spectra in AH model. As a reference, previous constraints by NANOGrav [14], EPTA [12] and PPTA [13] are simultaneously plotted. The parameters used here are explained in the text.

CMB bound [61, 62]. The brown line with $f_{\text{NG}} = 1$ is for comparison with the BOS model. We find it agrees with the spectrum depicted in the Fig. 6 of Ref. [50].

The spectrum of SGWB from BOS loops has a following structure. At high frequencies, the loops radiating in the RD era yields a plateau. At intermediate frequencies, a peak is created from GW emission from radiation-era loops in the matter era. Frequencies below $1/(G\mu_0)$ are suppressed since only small number of large loops can contribute. As investigated in Ref. [24], BOS model with $G\mu \lesssim 10^{-10}$ is favoured by the recent PTA experiments. In the AH model, however, f_{NG} suppresses the overall amplitude and hence $(G\mu, f_{\text{NG}}) = (10^{-8}, 0.1), (10^{-7}, 0.05)$ can be comparable to the BOS with $G\mu \simeq 10^{-10}$.

3 Multi-messenger measurements and its constraint on the AH string

Based on the above expressions of the energy injection into the visible sector and the SGWB, here we derive constraints on the AH model by applying the NANOGrav 12.5yr result [17] and the upper bound on the cascade energy density [47]. We also consider the BBN constraint on energy injection by decaying massive particles [46], finding that it is not substantially different from the DRGB constraint. Then we summarize the implications for this model, including the dark matter production based on Ref. [41], obtained by combining these multi-messenger constraints.

3.1 Big-Bang nucleosynthesis and gamma-ray constraints

As investigated in Ref. [40], an AH string network might alter the outcomes of Big-Bang Nucleosynthesis (BBN) and contribute the diffuse gamma-ray background (DGRB) through particle emission into the cosmic medium. Here we follow the discussion in Ref. [40] and

update the constraints on the AH string model, using the most recent BBN constraint on decaying massive (\gtrsim GeV) particles [46] and the upper bound on the cascade energy density [47].

The presence of long-lived massive particles decaying into SM species reduces the abundance of the light elements by dissociation due to hadronic and electromagnetic showers. Hence, the observed abundances of light elements puts bounds on the energy injection from those massive particles. In Ref. [46], the constraints are given in terms of $M_X Y_X$, where M_X is the mass of the new specie X (or the typical energy of emitted visible particles) and $Y_X \equiv n_X/s$ is its yield at times much less than than its lifetime τ_X . As discussed in Ref. [40], this bound can be applied to the energy density injected from the AH string network in one cosmic time $\Delta\rho_h = tQ_h(t)$ by making the approximate identification $M_X Y_X / \tau_X = Q_h/s$, and assuming that, for example via the emission of energetic SM Higgs, the SM particles produced by string decays are predominantly $b\bar{b}$. In other words, the AH string network is effectively a population of X particles decaying into $b\bar{b}$ at cosmic time t . Such an identification $\tau_X \sim t$ is possible because the lifetime of unstable SM particles is much shorter than the BBN time scale.

By using Eqs. (2.7)–(2.8) and the expression for the entropy density of the universe during RD era, we find

$$\frac{\Delta\rho_h(t)}{s(t)} \simeq 22\beta_{\text{SM}}^2 G\mu \left(\frac{m_p}{t}\right)^{1/2}, \quad (3.1)$$

where m_p is the Planck mass. Since the dominant decay channel of the SM Higgs is $h \rightarrow b\bar{b}$, the upper right panel of the Fig. 12 in Ref. [46] can be compared with Eq. (3.1). Then the strongest constraint on the string tension μ comes from Deuterium at $\tau_X \sim t \simeq 3 \times 10^3$ s as $M_X Y_X \sim \Delta\rho_h(t)/s(t) \lesssim 4 \times 10^{-14}$ GeV, which results in

$$G\mu \lesssim 3.6 \times 10^{-12} \beta_{\text{SM}}^{-2}. \quad (3.2)$$

Compared to the previous work [40], the constraint becomes tighter about an order of magnitude. This tightening is due to the refinement of the BBN constraint on decaying species by adopting newer constraints on the light elements abundance and improving calculation techniques (See Ref. [46] and references therein).

On the other hand, the DGRB measurement constrains the energy injection in the form of γ -rays in the late-time universe. In Ref. [47], the authors derives a bound on ω_{em} , the total energy density of cascade at the present epoch, from the latest Fermi-LAT measurement of DGRB at GeV scale [63]. This bound is given as

$$\omega_{\text{em}} \lesssim 8.3 \times 10^{-8} \text{eV/cm}^3, \quad (3.3)$$

which is again about an order of magnitude reduction from the value used in Ref. [40]. Denoting the fraction of the energy of the string decay products that end up in γ -rays around GeV scale as f_{em} , $\omega_{\text{em}}(t)$ in the late-time universe can be expressed as

$$\omega_{\text{em}}(t) = f_{\text{em}} \Delta\rho_h(t) \simeq 0.5 f_{\text{em}} \beta_{\text{SM}}^2 \frac{\mu}{t^2}, \quad (3.4)$$

where the MD era expression of Eq. (2.8) is used for $\Delta\rho_h(t)$. Again assuming that the decay products from strings are dominated by the SM Higgs, many photons are produced via pion

decays originated from the primary decay channel of Higgs: $h \rightarrow b\bar{b}$. This naturally leads to $f_{\text{em}} \sim 1$ and one can derive the constraint for the string tension as

$$G\mu \lesssim 4 \times 10^{-12} \beta_{\text{SM}}^{-2}. \quad (3.5)$$

Here we use only 1 significant digit because of order of magnitude estimate on the additional parameter f_{em} . Nevertheless, $f_{\text{em}} \ll 1$ should be unlikely since photons will also be produced by charged particle interactions that take place in the cosmological plasma [64]. We should note that the both constraints depend on the details of the coupling of the string sector fields and the visible sector, but are in principle calculable once the field theory is specified. In the following, we will use the constraint from the DGRB (3.5) to give a more conservative estimate.

3.2 Mapping the NANOGrav 12.5yr result

Pulsar Timing Array experiments have recently reported strong evidence for a common-spectrum stochastic process [17–20], which might be a signal of a nanohertz SGWB. Here we investigate the possibility that the origin of this common stochastic process is the SGWB from the NG-like loops in the AH string network.

In the analysis performed by the NANOGrav collaboration [17], the SGWB is modeled as a power-law around a reference frequency $f_{\text{yr}} = 1 \text{ yr}$ as

$$h_c^{(\text{pow})}(f) = A \left(\frac{f}{f_{\text{yr}}} \right)^{(3-\gamma)/2}, \quad (3.6)$$

which is expressed in terms of the spectral GW energy density as

$$\Omega_{\text{gw}}^{(\text{pow})}(f) = \frac{2\pi^2}{3H_0^2} f^2 h_c^{(\text{pow})2}(f) = \frac{2\pi^2}{3H_0^2} A^2 f_{\text{yr}}^2 \left(\frac{f}{f_{\text{yr}}} \right)^{5-\gamma}. \quad (3.7)$$

In Fig. 2, the 68% and 95% posterior likelihood contours from the NANOGrav result are plotted in part of the $\gamma - A$ plane.

To connect this result with the SGWB from cosmic strings, we need construct a map between the power-law fit parameters (γ, A) and the cosmic string parameters $(G\mu, f_{\text{NG}})$. In previous works, this was accomplished by fitting the theoretical cosmic string spectra with power laws. Here we adopt a method based on Ref. [65]. This takes into account the fact that spectra which are not exactly power laws are being observed by an instrument with a frequency-dependent noise, and so a simple least-squares fit will be biased.

Assuming Gaussian noise and the Gaussian SGWB from the AH strings, the likelihood of the data x is given as

$$P(x|S_{\text{gw}}^{(\text{AH})}) = \prod_{f_i \in [f_{\text{min}}, f_{\text{max}}]} \frac{2T_{\text{obs}}}{(2\pi)^{1/2} \left[S_n(f_i) + S_{\text{gw}}^{(\text{AH})}(f_i) \right]} \exp \left(-\frac{T_{\text{obs}} |\tilde{x}(f_i)|^2}{S_n(f_i) + S_{\text{gw}}^{(\text{AH})}(f_i)} \right), \quad (3.8)$$

where $S_n(f)$ is the effective strain noise spectral density and $S_{\text{gw}}^{(\text{AH})}(f) = (3H_0^2/2\pi^2 f^3) \Omega_{\text{gw}}^{(\text{AH})}(f)$ is the spectral density of the SGWB from the cosmic strings. In this study, we identify $S_n(f)$ as the effective sensitivity of the 12.5 yr NANOGrav estimated by a python code `Hasasia` [66], which is presented in, for example, the page 10 of Ref. [67]. Assuming a flat prior distribution

$P(S_{\text{gw}}^{(\text{pow})}(A, \gamma))$, the likelihood for the power-law fitting with given data is modeled in the same way:

$$P(S_{\text{gw}}^{(\text{pow})}|x) \propto P(x|S_{\text{gw}}^{(\text{pow})})P(S_{\text{gw}}^{(\text{pow})}) \\ \propto \prod_{f_i \in [f_{\text{min}}, f_{\text{max}}]} \frac{2T_{\text{obs}}}{(2\pi)^{1/2} [S_n(f_i) + S_{\text{gw}}^{(\text{pow})}(f_i)]} \exp \left(-\frac{T_{\text{obs}}|\tilde{x}(f_i)|^2}{S_n(f_i) + S_{\text{gw}}^{(\text{pow})}(f_i)} \right), \quad (3.9)$$

where $S_{\text{gw}}^{(\text{pow})}(f) = (3H_0^2/2\pi^2 f^3)\Omega_{\text{gw}}^{(\text{pow})}(f)$. By marginalizing over the data in frequency space, the likelihood function, which quantifies how probable the power-law fitting (γ, A) is for the SGWB from the strings with a given $(G\mu, f_{\text{NG}})$, is constructed as

$$P(S_{\text{gw}}^{(\text{pow})}|S_{\text{gw}}^{(\text{AH})}) = \int dx P(S_{\text{gw}}^{(\text{pow})}|x)P(x|S_{\text{gw}}^{(\text{AH})}) \\ \propto \prod_{f_i \in [f_{\text{min}}, f_{\text{max}}]} \frac{\sqrt{[S_n(f_i) + S_{\text{gw}}^{(\text{pow})}(f_i)][S_n(f_i) + S_{\text{gw}}^{(\text{AH})}(f_i)]}}{[S_n(f_i) + S_{\text{gw}}^{(\text{pow})}(f_i)] + [S_n(f_i) + S_{\text{gw}}^{(\text{AH})}(f_i)]}. \quad (3.10)$$

Each string GWB spectrum can be fitted by the power-law parameters (γ, A) which maximize this likelihood function. This defines a map from $(G\mu, f_{\text{NG}})$ to (γ, A) . We take five frequency bins ($f_{\text{min}}, 2f_{\text{min}}, \dots, 5f_{\text{min}}$) in our analysis with $f_{\text{min}} = 12.5$ yr, which are the same bins analyzed by the NANOGrav for the power-law fitting.

In Fig. 2, we compare our method to the simple numerical fitting and the two lowest frequency bin fitting adopted in Ref. [24], for $G\mu = 10^{-10}$ and $f_{\text{NG}} = 1$. The authors in

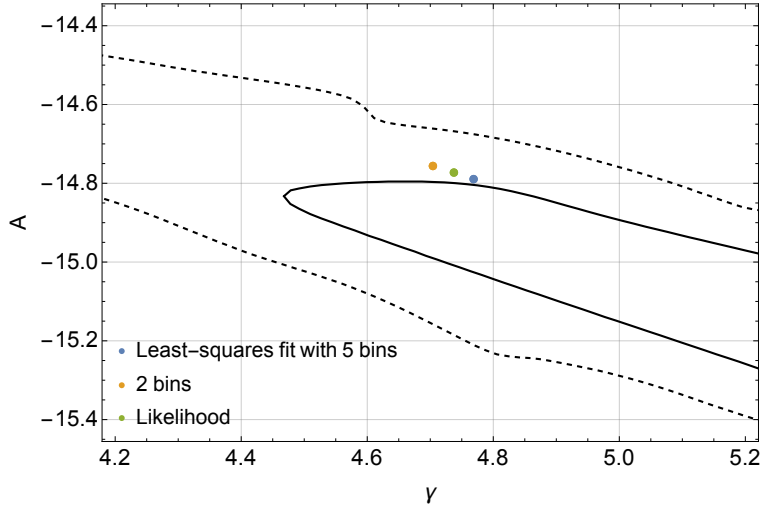


Figure 2. 68% and 95% posterior likelihood contours from NANOGrav data, and comparison between the different fitting methods with $G\mu = 10^{-10}$ and $f_{\text{NG}} = 1$. Due to the weight taking into account the noise power, our fitting (green) lies in between the five bin numerical fitting (blue) and the lowest two bin fitting (orange).

Ref. [24] select those two bins since the noise contribution is expected to be the smallest there. This can be understood as the extreme limit of our fitting method, which is weighted

by the relative size of the signal power to the modeled noise power. Thus, it is reasonable that the result of our fitting is in between the lowest two bin fitting and the numerical fitting which evenly weights the five bins. While the difference of the fitting methods seems not so significant, we use our likelihood model throughout this study to avoid the bias as much as possible.

With this likelihood model, we can construct the inverse map from the space (γ, A) to $(G\mu, f_{\text{NG}})$, and hence the image of NANOGrav power-law contours in the $G\mu - f_{\text{NG}}$ plane as follows. We first scan over the sets of string loop parameters $(G\mu, f_{\text{NG}})$ and find the corresponding power-law parameters (γ, A) by maximizing the likelihood (3.10) as demonstrated in the left panel of Fig. 3. We divide the range of $G\mu$ into two sections $[2 \times 10^{-11}, 3 \times 10^{-10}]$ and $[3 \times 10^{-10}, 10^{-7}]$, both are sampled into 25 logarithmically spaced values. f_{NG} is also logarithmically sampled into 25 values over $10^{-2} \leq f_{\text{NG}} \leq 1$ for each of them in the former segment, and $3 \times 10^{-3} \leq f_{\text{NG}} \leq 0.3$ for the latter segment. Hence, we have $2 \times 25 \times 25$ points in total. With these sampling points mapped through the likelihood, the points in the $G\mu - f_{\text{NG}}$ plane, which correspond to the points (γ_c, A_c) on the NANOGrav contours, can be estimated. This is the reason why we call the “inverse map” to $G\mu - f_{\text{NG}}$ plane. In this work, we use the following estimator [65] weighted by the Euclidean distance in the mapped parameter space:

$$\bar{X} = \left(\sum_{i=1}^N \frac{1}{d_i} \right)^{-1} \sum_{i=1}^N \frac{X_i}{d_i}, \quad (3.11)$$

where $d_i = \sqrt{(\gamma_i - \gamma_c)^2 + (A_i - A_c)^2}$ is the distance between the point of interest (γ_c, A_c) and the sampling points (γ_i, A_i) mapped from the string parameters $X_i = (G\mu_i, f_{\text{NG}i})$. N is the number of the sampling points closest to (γ_c, A_c) , which is used in estimating the inverse map of (γ_c, A_c) , namely $\bar{X} = (\bar{G\mu}, \bar{f}_{\text{NG}})$. Note that, due to the characteristics of the spectrum discussed at the end of Sec. 2.2, there can be two different values of $(G\mu, f_{\text{NG}})$ that are fitted to the same (γ, A) . In the left panel of Fig. 3, blue dots represent the mapping of points with $f_{\text{NG}} = 1$ while $G\mu$ is varied from left (smaller) to right (larger). Though A monotonically increases with $G\mu$, γ starts to decrease around the curve at $\gamma \simeq 5.15$ corresponding to $G\mu \simeq 5 \times 10^{-9}$. On the other hand, lowering the value of f_{NG} with fixed $G\mu$ (orange dots in the left panel of Fig. 3) results in decreasing A almost without changing γ since it controls the overall amplitude of $\Omega_{\text{gw}}^{(\text{AH})}$. From these observations, one can deduce that, by changing f_{NG} , degeneracy occurs between the two branches $5 \times 10^{-10} \lesssim G\mu \lesssim 5 \times 10^{-9}$ and $5 \times 10^{-9} \lesssim G\mu \lesssim 10^{-7}$ reside in $\gamma \gtrsim 5$. This indicates that we may overlook some set of the string parameters if we simply maximize the likelihood with respect to a specific (γ_c, A_c) .

The estimator (3.11) can be easily implemented to systematically obtain a correct image of the NANOGrav contours while dealing with the degeneracy mentioned above. First, we scan the different values of f_{NG} with a fixed value of $G\mu$ as orange dots in the left panel of Fig. 3 and find the intersections (γ_c, A_c) between the interpolation of these sampling points and the contours. Then we choose two closest sampling points (γ_i, A_i) for each intersection to estimate the value of $(\bar{G\mu}, \bar{f}_{\text{NG}})$ that would correspond to (γ_c, A_c) . From Eq. (3.11) with $N = 2$, we can estimate the value of \bar{f}_{NG} as

$$\bar{f}_{\text{NG}} = \left(\frac{1}{d_1} + \frac{1}{d_2} \right)^{-1} \left(\frac{f_{\text{NG}1}}{d_1} + \frac{f_{\text{NG}2}}{d_2} \right), \quad (3.12)$$

where $f_{\text{NG}1}$ and $f_{\text{NG}2}$ represent the value of f_{NG} of the two closest points, and the distance can be well approximated by $d_i \simeq |A_i - A_c|$. Note that $\bar{G\mu}$ is immediately identified with

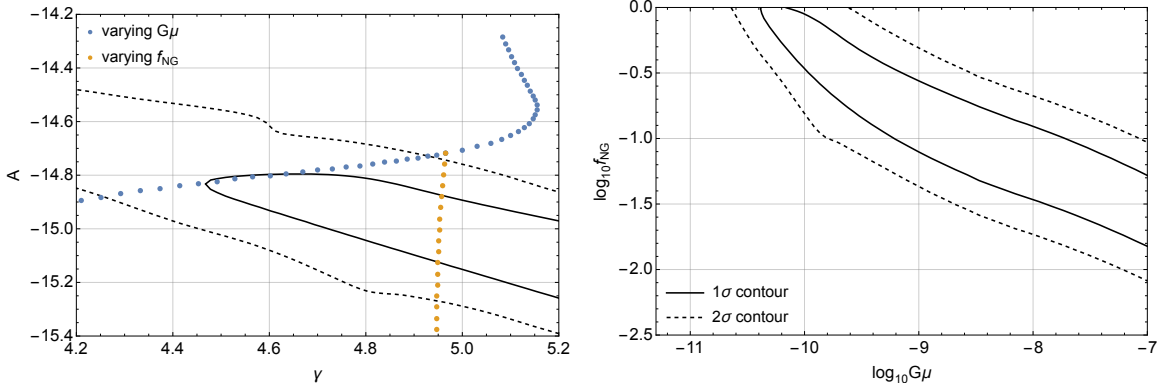


Figure 3. (Left panel) Variation of the AH string parameters $(G\mu, f_{\text{NG}})$ in the $\gamma - A$ plane is shown. Blue dots correspond to $f_{\text{NG}} = 1$ and $G\mu$ is logarithmically varied from $G\mu = 10^{-7}$ to $G\mu = 3 \times 10^{-10}$, and from $G\mu = 3 \times 10^{-10}$ to $G\mu = 2 \times 10^{-11}$. Orange dots correspond to $G\mu = 3 \times 10^{-10}$ and here f_{NG} is logarithmically varied from $f_{\text{NG}} = 1$ to $f_{\text{NG}} = 0.07$. (Right panel) The mapping of the power-law fitting from the NANOGrav 12.5yr results. Here the black(-dashed) line represents contours of 68% (95%) confidence.

$G\mu$ since the sampling points with fixed $G\mu$ are concerned. We repeat this procedure for different values of $G\mu$ to obtain a set of inversely mapped points on the $G\mu - f_{\text{NG}}$ plane. Importantly, this procedure performed on each value of $G\mu$ allows us to deal with parameters degenerate in $\gamma - A$ plane. By smoothly connecting these points, the global shape of contours are depicted in the $G\mu - f_{\text{NG}}$ plane as shown in the right panel of Fig. 3.

To refine the shape, additional points, for example, the bending of the 65% confidence contour around $\gamma \simeq 4.5$ are also inversely mapped. In this case, the four closest sampling points were used to determine both $\overline{G\mu}$ and \overline{f}_{NG} through Eq. (3.11) with $N = 4$. Note that these points are free from the degeneracy, the value of $\overline{G\mu}$ can be correctly estimated with sufficiently small spacing of the sampling points. As a check of the method, we confirmed that the contours in the power-law parameter space (γ_c, A_c) are reproduced within 1% errors by maximizing the likelihood (3.10) with respect to the estimated string parameters $(\overline{G\mu}, \overline{f}_{\text{NG}})$.

Note that the mapped contours should be regarded as an approximation of the true 68% and 95% contours of posterior likelihood in the $(G\mu, f_{\text{NG}})$ space arising from the NANOGrav result. A more rigorous approach would construct the posterior with a Markov chain Monte Carlo method, sampling directly on the parameters $(G\mu, f_{\text{NG}})$, with a physically motivated prior, using the likelihood function of the observations. Even without performing such runs, our method could be improved by using the chains constructed from sampling on the (γ, A) space, and reweighting according to the prior induced by the mapping between the two parameter spaces [65].

3.3 Combined constraints and implications for the AH model

Here we combine the constraints from the NANOGrav 12.5 yr data and the DGRB observations by Fermi-LAT with the Planck CMB upper bound $G\mu \lesssim 10^{-7}$ and the constraint $f_{\text{NG}} \lesssim 0.1$ from simulations to investigate the allowed parameter region of the AH model [61, 62]. These constraints are summarised in Fig. 4. In the region $f_{\text{NG}} \lesssim 0.1$ and $G\mu \lesssim 10^{-7}$, the lower branches of the likelihood contours from NANOGrav can be approxi-

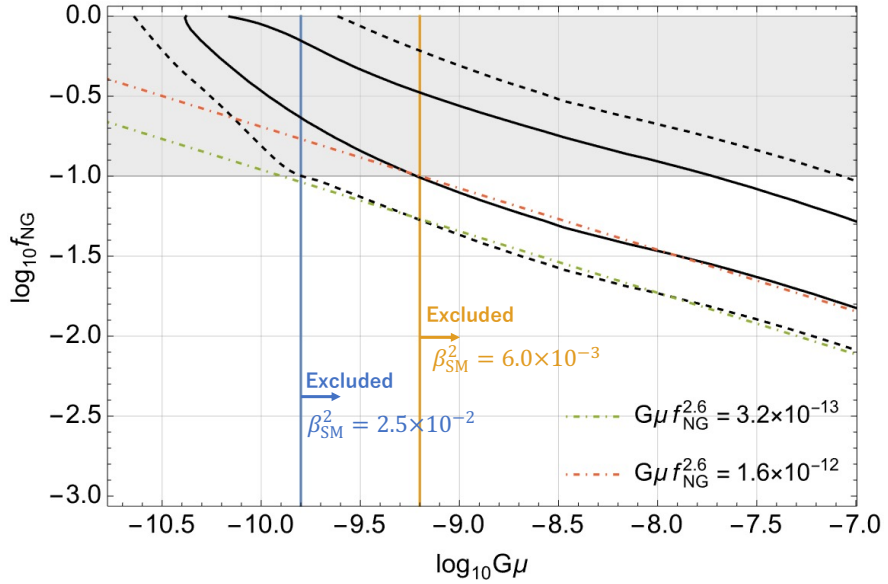


Figure 4. Constraints on AH string model parameters which allow an explanation of the NANOGrav result, while satisfying constraints from numerical simulations and the DGRB. The mapped NANOGrav 68% and 95% likelihood contours are shown as solid black and dashed black lines. The lower branch of each contour is approximated by the dot-dashed lines with constant $G\mu f_{\text{NG}}^{2.6}$ in the region $f_{\text{NG}} \lesssim 0.1$ and $G\mu \lesssim 10^{-7}$. The region excluded by the upper bound on the fraction of NG-like loops $f_{\text{NG}} \lesssim 0.1$ from numerical simulations [39] is indicated by grey shading. The blue and orange solid lines correspond to the lowest values of $G\mu$ required to explain the NANOGrav result that are within the 65% and 95% confidence regions. The annotation with the same color illustrates the DGRB constraint (3.5) on the fractional energy of the strings going into Standard Model particles β_{SM}^2 , where those values of $G\mu$ become the maximally allowed value.

mately characterised as

$$G\mu f_{\text{NG}}^{2.6} \gtrsim 3.2 \times 10^{-13} \text{ (95\%)}, \quad G\mu f_{\text{NG}}^{2.6} \gtrsim 1.6 \times 10^{-12} \text{ (68\%)}, \quad (3.13)$$

which are plotted as the colored dot-dashed line. One can see that the AH model should have $f_{\text{NG}} \gtrsim 0.01$ in order for there to exist string tensions within the 95% confidence region which satisfy the CMB constraint. This bound is a factor of 10 larger than the rough estimate in the previous study [39], due to our more careful analysis. Such a lower bound on the value of f_{NG} provides an experimentally motivated target for the numerical simulation of the AH string loops.

In addition, the string field needs to be sufficiently “dark”, or sequestered from the visible sector, if AH strings are to explain the NANOGrav result. The colored vertical lines in Fig. 4 indicates the lowest values of the string tension within the 65% and 95% confidence regions of parameter space accounting for the NANOGrav result, where the exclusion of $f_{\text{NG}} \gtrsim 0.1$ is taken into account. In order for such values of string tension to satisfy the DRGB constraint (3.5), in which the maximally allowed value of $G\mu$ monotonically increases with decreasing β_{SM} , β_{SM} needs to be bounded from above. A string tension $\log_{10} G\mu \gtrsim -9.8$ is required to reach the 95% confidence region, which in turn requires $\beta_{\text{SM}}^2 \lesssim 3 \times 10^{-2}$ in order for AH strings to satisfy the DRGB bound while accounting for the NANOGrav signal. At 65% confidence, a string tension $\log_{10} G\mu \gtrsim -9.2$ is required, which implies $\beta_{\text{SM}}^2 \lesssim 6 \times 10^{-3}$.

Let us further discuss the implications of our result for the AH model. The decay products of the massive radiation from the AH string network should end up distributed between SM particles, dark matter and dark radiation. If we characterize this branching ratio of the energy density as β_{DM}^2 and β_{DR}^2 , in the same way as β_{SM}^2 , $\beta_{\text{SM}}^2 + \beta_{\text{DM}}^2 + \beta_{\text{DR}}^2 \lesssim 1$ should be satisfied.⁵ As discussed in the above, $\beta_{\text{SM}}^2 < 0.03$, or $\beta_{\text{DM}}^2 + \beta_{\text{DR}}^2 > 0.97$ is required for the AH string to explain NANOGrav result. While the decay into the dark radiation cannot be tightly constrained, the dark matter (DM) production from the strings can give a constraint on the new string parameters.

For example, Ref. [41] considers production of TeV scale DM χ from decaying cosmic strings via the intermediate state X . There its mass was assumed as $m_\chi = 500$ GeV for the concreteness and we also assume it in the following. The constraints are summarized in the Table 2 of Ref. [41] and here we briefly discuss its application. Assuming the standard freeze-out scenario, it was shown that cosmic strings in the AH model (referred to as the field theory scenario) can be a principal source of DM. In this case, the relic abundance depends on the energy injection characterized by $G\mu\beta_{\text{DM}}^2$ in the same way as⁶ Eqs. (2.7)–(2.8) and on $\sigma_0 \equiv \langle \sigma_\chi v \rangle|_{T=m_\chi}$, which is the thermally averaged DM annihilation cross section at the temperature equal to DM mass m_χ . Hence, depending on whether s-wave or p-wave annihilation is dominant, relic DM abundance measured by Planck gives the upper bound on this injection and hence a bound on $G\mu$ as

$$G\mu \lesssim \begin{cases} 1 \times 10^{-9} \beta_{\text{DM}}^{-2} (\sigma_0/10^{-23} \text{cm}^3 \text{s}^{-1}) & (\text{s-wave}) \\ 7 \times 10^{-12} \beta_{\text{DM}}^{-2} (\sigma_0/10^{-23} \text{cm}^3 \text{s}^{-1})^{1/2} & (\text{p-wave}), \end{cases} \quad (3.14)$$

where equality corresponds to the case where observed amount of DM is reproduced by the string decay. To account for the relic DM abundance simultaneously for the NANOGrav signal, which favours larger value of $G\mu$, smaller values of β_{DM} and σ_0 might be required from Eq. (3.14). However, one cannot increase the annihilation cross section arbitrarily due to unitarity [68]. This unitarity bound on the cross section can be recast for our reference value of $m_\chi = 500$ GeV as

$$G\mu \lesssim \begin{cases} 2 \times 10^{-7} \beta_{\text{DM}}^{-2} & (\text{s-wave}) \\ 8 \times 10^{-10} \beta_{\text{DM}}^{-2} & (\text{p-wave}), \end{cases} \quad (3.15)$$

where equality in Eq. (3.14) is assumed. One can quickly establish that accounting for the NANOGrav result with a larger $G\mu$ does lead to a constraint on the DM decay fraction for p-wave dominance. For example, $G\mu \simeq 10^{-8}$ can yield the correct DM relic abundance without violating p-wave unitarity only if $\beta_{\text{DM}}^2 \lesssim 0.1$. In this case, to avoid the DGRB constraint, most of the AH string decay products should then end up in the form of dark radiation as $\beta_{\text{DR}}^2 \gtrsim 0.9$.

For s-wave dominance, a constraint from the Fermi-LAT observation of γ -ray in dwarf spheroidal satellite galaxies [69] is also considered in Ref. [41]. This gives $G\mu \lesssim 10^{-10} \beta_{\text{DM}}^{-2}$ and again smaller β_{DM}^2 (and larger β_{DR}^2 to avoid the DGRB constraint) is required for AH strings which account for the NANOGrav signal with a larger $G\mu$.

⁵Note that this sum is slightly less than 1 due to the GW emission from the NG-like loops for the values of f_{NG} of our interest.

⁶Here we can effectively identify β_{DM}^2 with f_X in Ref. [41]. Then P_{FT} in Ref. [41] can be expressed as $P_{\text{FT}} \simeq 8.9 \times 10^{-2} \beta_{\text{DM}}^2$ for RD era.

In this way, the branching ratio of the AH string decay products can be investigated for a specific model. Although it generally depends on details of the DM, such constraints on this ratio have an important implication to how the AH model should be embedded in the model of particle physics. The intriguing possibility that strings in a particular model could account for significant fractions of the NANOGrav signal, the Fermi-LAT measurement of the DRGB, and the dark matter is still open.

4 Discussion

In this study, we investigated the Abelian-Higgs model in light of recent results of PTA experiments which can be interpreted in terms of a stochastic gravitational wave background. Motivated by the recent simulation of the AH string loops [39, 42], we consider the possibility that AH strings radiate both particles and gravitational waves. By introducing parameters f_{NG} , β_{SM}^2 , β_{DM}^2 , and β_{DR}^2 we characterize these two classes of signals from the AH string network. The parameter f_{NG} accounts for the uncertainty in the understanding of the NG-like loop production in the AH model, while the parameters β_{SM}^2 , β_{DM}^2 , and β_{DR}^2 are the model-dependent fractional energies of the string network appearing as Standard Model particles, dark matter, and dark radiation. The decay fraction β_{SM}^2 is bounded by the diffuse γ -ray background observations of Fermi-LAT and by the bounds on dissociation of light elements during Big Bang nucleosynthesis.

We modelled the uncertainty by supposing that a fraction of the AH string loops are NG-like and follow the loop distribution inferred from NG simulations [49], leading to a SGWB a factor f_{NG} smaller than the NG prediction. The improvement of the GWB estimation can be achieved when the further understanding of the NG-like loop production is established. Such a refinement may allow us to precisely probe AH model by the multi-band GWB observation including ground-based detectors and space-based detectors.

Then we probed the allowed parameter region of the AH strings by combining the constraints on gravitational wave production from NANOGrav [17] with updated constraints on particle production from the DGRB and BBN. In practice, the particle production constraints are very similar and we used only the DGRB. In contrast to the previous studies on the cosmic string interpretation of the NANOGrav result, which simply fitted the SGWB from the cosmic strings by a power-law, we model the likelihood function for the AH string parameters, which has the advantage of avoiding a possible bias in the posterior. By maximizing this likelihood function, we map the sets of string parameters to the power-law parameter space. By inverting the map, we reconstruct the NANOGrav likelihood contours in the string parameter space. We find that, to account for the NANOGrav result with approximately 95% confidence, while respecting the CMB bound on the string tension $G\mu \lesssim 10^{-7}$ and the simulation bound on the NG-like loop fraction $f_{\text{NG}} \lesssim 0.1$, the combination $G\mu f_{\text{NG}}^{2.6} \gtrsim 3.2 \times 10^{-13}$ (95%) is required. From this, the DGRB bound on $G\mu$ implies an upper bound on SM decay fraction as $\beta_{\text{SM}}^2 < 0.03$, which indicates that more than 97% of the total network energy should end up in the form of dark matter or dark radiation. Interestingly, there is a possibility that the observed relic DM abundance can be explained by a specific AH model satisfying all the constraints mentioned above.

Due to the suppression of the GWB amplitude by f_{NG} , a higher value of the string tension is still viable for AH strings and the relatively high scale symmetry-breaking might be possible, up to the CMB bound $G\mu \lesssim 10^{-7}$. If the fraction of NG-like loops is sufficiently low, $f_{\text{NG}} \lesssim 0.01$, the NANOGrav result cannot be explained by AH strings. Establishing

whether the upper limit on f_{NG} is lower than this value motivates large-scale numerical simulation of AH loop production.

For AH strings which do account for the NANOGrav signal, the resulting bound on the decay fraction into SM particles $\beta_{\text{SM}}^2 < 0.03$ motivates the exploration of models where the string fields are weakly coupled to the SM. In the context of such SM extensions, one may further discuss decays into dark matter and dark radiation, and the constraints on β_{DM} and β_{DR} . In this way, multi-messenger investigation can provide information SM extensions with spontaneously broken U(1) symmetries. However, since the evidence of SGWB detection is not conclusive in the present PTA results, we should carefully follow future results and analysis.

The extension of our study can be considered in the following directions. First, relation between the decay fraction parameters $\beta_{\text{SM}}, \beta_{\text{DM(R)}}$ and f_{NG} can be investigated. While we have treated them independently, these parameters can be related to each other through the scaling of the network which is maintained by the particle emission and NG-like loop production. This will require a clearer understanding of loop production in AH model. Second, it will be interesting to translate the DGRB and BBN bounds into the constraints on the parameters in the Lagrangian of specific models. This motivates investigation of the dependence of β_{SM} and $\beta_{\text{DM(R)}}$ on coupling constants. It will be also interesting to investigate other models of cosmic string in this multi-messenger context. For example, our results are particularly relevant for $B - L$ strings [45, 70, 71], although all the constraints we consider can be avoided if the U(1) symmetry is embedded in a larger symmetry group so that the strings are metastable [72]. In such models strong SGWBs can be produced at early times, and be observable at LISA and other instruments [72], without violating any of the constraints discussed here.

Acknowledgments

The authors would like to thank Takeo Moroi for useful comments on the BBN constraint. JK (ORCID ID 0000-0003-3126-5100) is supported by JSPS KAKENHI, Grant-in-Aid for JSPS Fellows 20J21866 and research program of the Leading Graduate Course for Frontiers of Mathematical Sciences and Physics (FMSP). JK thanks the Helsinki Institute of Physics for hosting his visit to conduct this project and also for their hospitality. MH (ORCID ID 0000-0002-9307-437X) acknowledges support from the Academy of Finland grant no. 333609.

References

- [1] A. Vilenkin and E. P. S. Shellard, *Cosmic strings and other topological defects*. Cambridge monographs on mathematical physics. Cambridge Univ. Press, Cambridge, 1994.
- [2] M. B. Hindmarsh and T. W. B. Kibble, *Cosmic strings*, *Rept. Prog. Phys.* **58** (1995) 477–562, [[hep-ph/9411342](#)].
- [3] M. Hindmarsh, *Signals of Inflationary Models with Cosmic Strings*, *Prog. Theor. Phys. Suppl.* **190** (2011) 197–228, [[1106.0391](#)].
- [4] E. J. Copeland, L. Pogosian and T. Vachaspati, *Seeking String Theory in the Cosmos*, *Class. Quant. Grav.* **28** (2011) 204009, [[1105.0207](#)].
- [5] D. Forster, *Dynamics of Relativistic Vortex Lines and their Relation to Dual Theory*, *Nucl. Phys. B* **81** (1974) 84–92.

[6] H. Arodz, *Expansion in the width: The case of vortices*, *Nucl. Phys. B* **450** (1995) 189–208, [[hep-th/9503001](#)].

[7] M. R. Anderson, F. Bonjour, R. Gregory and J. Stewart, *Effective action and motion of a cosmic string*, *Phys. Rev. D* **56** (1997) 8014–8028, [[hep-ph/9707324](#)].

[8] E. P. S. Shellard, *Cosmic String Interactions*, *Nucl. Phys. B* **283** (1987) 624–656.

[9] R. A. Matzner, *Interaction of $U(1)$ cosmic strings: Numerical intercommutation*, *Comput. Phys.* **2** (1988) 51–64.

[10] A. Achucarro and R. de Putter, *Effective non-intercommutation of local cosmic strings at high collision speeds*, *Phys. Rev. D* **74** (2006) 121701, [[hep-th/0605084](#)].

[11] P. Auclair et al., *Probing the gravitational wave background from cosmic strings with LISA*, *JCAP* **04** (2020) 034, [[1909.00819](#)].

[12] L. Lentati et al., *European Pulsar Timing Array Limits On An Isotropic Stochastic Gravitational-Wave Background*, *Mon. Not. Roy. Astron. Soc.* **453** (2015) 2576–2598, [[1504.03692](#)].

[13] R. M. Shannon et al., *Gravitational waves from binary supermassive black holes missing in pulsar observations*, *Science* **349** (2015) 1522–1525, [[1509.07320](#)].

[14] NANOGrav collaboration, Z. Arzoumanian et al., *The NANOGrav 11-year Data Set: Pulsar-timing Constraints On The Stochastic Gravitational-wave Background*, *Astrophys. J.* **859** (2018) 47, [[1801.02617](#)].

[15] J. J. Blanco-Pillado, K. D. Olum and X. Siemens, *New limits on cosmic strings from gravitational wave observation*, *Phys. Lett. B* **778** (2018) 392–396, [[1709.02434](#)].

[16] C. Ringeval and T. Suyama, *Stochastic gravitational waves from cosmic string loops in scaling*, *JCAP* **12** (2017) 027, [[1709.03845](#)].

[17] NANOGrav collaboration, Z. Arzoumanian et al., *The NANOGrav 12.5 yr Data Set: Search for an Isotropic Stochastic Gravitational-wave Background*, *Astrophys. J. Lett.* **905** (2020) L34, [[2009.04496](#)].

[18] B. Goncharov et al., *On the Evidence for a Common-spectrum Process in the Search for the Nanohertz Gravitational-wave Background with the Parkes Pulsar Timing Array*, *Astrophys. J. Lett.* **917** (2021) L19, [[2107.12112](#)].

[19] S. Chen et al., *Common-red-signal analysis with 24-yr high-precision timing of the European Pulsar Timing Array: inferences in the stochastic gravitational-wave background search*, *Mon. Not. Roy. Astron. Soc.* **508** (2021) 4970–4993, [[2110.13184](#)].

[20] J. Antoniadis et al., *The International Pulsar Timing Array second data release: Search for an isotropic gravitational wave background*, *Mon. Not. Roy. Astron. Soc.* **510** (2022) 4873–4887, [[2201.03980](#)].

[21] J. Ellis and M. Lewicki, *Cosmic String Interpretation of NANOGrav Pulsar Timing Data*, *Phys. Rev. Lett.* **126** (2021) 041304, [[2009.06555](#)].

[22] S. Blasi, V. Brdar and K. Schmitz, *Has NANOGrav found first evidence for cosmic strings?*, *Phys. Rev. Lett.* **126** (2021) 041305, [[2009.06607](#)].

[23] W. Buchmuller, V. Domcke and K. Schmitz, *From NANOGrav to LIGO with metastable cosmic strings*, *Phys. Lett. B* **811** (2020) 135914, [[2009.10649](#)].

[24] J. J. Blanco-Pillado, K. D. Olum and J. M. Wachter, *Comparison of cosmic string and superstring models to NANOGrav 12.5-year results*, *Phys. Rev. D* **103** (2021) 103512, [[2102.08194](#)].

[25] L. Bian, R.-G. Cai, J. Liu, X.-Y. Yang and R. Zhou, *Evidence for different gravitational-wave sources in the NANOGrav dataset*, *Phys. Rev. D* **103** (2021) L081301, [[2009.13893](#)].

[26] Z.-C. Chen, Y.-M. Wu and Q.-G. Huang, *Search for the Gravitational-wave Background from Cosmic Strings with the Parkes Pulsar Timing Array Second Data Release*, [2205.07194](#).

[27] L. Bian, J. Shu, B. Wang, Q. Yuan and J. Zong, *Searching for cosmic string induced stochastic gravitational wave background with the Parkes Pulsar Timing Array*, [2205.07293](#).

[28] H. B. Nielsen and P. Olesen, *Vortex Line Models for Dual Strings*, *Nucl. Phys. B* **61** (1973) 45–61.

[29] G. Vincent, N. D. Antunes and M. Hindmarsh, *Numerical simulations of string networks in the Abelian Higgs model*, *Phys. Rev. Lett.* **80** (1998) 2277–2280, [[hep-ph/9708427](#)].

[30] J. N. Moore, E. P. S. Shellard and C. J. A. P. Martins, *On the evolution of Abelian-Higgs string networks*, *Phys. Rev. D* **65** (2002) 023503, [[hep-ph/0107171](#)].

[31] N. Bevis, M. Hindmarsh, M. Kunz and J. Urrestilla, *CMB power spectrum contribution from cosmic strings using field-evolution simulations of the Abelian Higgs model*, *Phys. Rev. D* **75** (2007) 065015, [[astro-ph/0605018](#)].

[32] N. Bevis, M. Hindmarsh, M. Kunz and J. Urrestilla, *CMB power spectra from cosmic strings: predictions for the Planck satellite and beyond*, *Phys. Rev. D* **82** (2010) 065004, [[1005.2663](#)].

[33] D. Daverio, M. Hindmarsh, M. Kunz, J. Lizarraga and J. Urrestilla, *Energy-momentum correlations for Abelian Higgs cosmic strings*, *Phys. Rev. D* **93** (2016) 085014, [[1510.05006](#)].

[34] J. R. C. C. C. Correia and C. J. A. P. Martins, *Extending and Calibrating the Velocity dependent One-Scale model for Cosmic Strings with One Thousand Field Theory Simulations*, *Phys. Rev. D* **100** (2019) 103517, [[1911.03163](#)].

[35] J. R. C. C. C. Correia and C. J. A. P. Martins, *Quantifying the effect of cooled initial conditions on cosmic string network evolution*, *Phys. Rev. D* **102** (2020) 043503, [[2007.12008](#)].

[36] J. R. C. C. C. Correia and C. J. A. P. Martins, *Abelian–Higgs cosmic string evolution with multiple GPUs*, *Astron. Comput.* **34** (2021) 100438, [[2005.14454](#)].

[37] M. Hindmarsh, A. Kormu, A. Lopez-Eiguren and D. J. Weir, *Scaling in necklaces of monopoles and semipoles*, *Phys. Rev. D* **98** (2018) 103533, [[1809.03384](#)].

[38] M. Hindmarsh, S. Stuckey and N. Bevis, *Abelian Higgs Cosmic Strings: Small Scale Structure and Loops*, *Phys. Rev. D* **79** (2009) 123504, [[0812.1929](#)].

[39] M. Hindmarsh, J. Lizarraga, A. Urio and J. Urrestilla, *Loop decay in Abelian-Higgs string networks*, *Phys. Rev. D* **104** (2021) 043519, [[2103.16248](#)].

[40] H. F. Santana Mota and M. Hindmarsh, *Big-Bang Nucleosynthesis and Gamma-Ray Constraints on Cosmic Strings with a large Higgs condensate*, *Phys. Rev. D* **91** (2015) 043001, [[1407.3599](#)].

[41] M. Hindmarsh, R. Kirk and S. M. West, *Dark Matter from Decaying Topological Defects*, *JCAP* **03** (2014) 037, [[1311.1637](#)].

[42] D. Matsunami, L. Pogosian, A. Saurabh and T. Vachaspati, *Decay of Cosmic String Loops Due to Particle Radiation*, *Phys. Rev. Lett.* **122** (2019) 201301, [[1903.05102](#)].

[43] T. Vachaspati, *Cosmic Rays from Cosmic Strings with Condensates*, *Phys. Rev. D* **81** (2010) 043531, [[0911.2655](#)].

[44] T. W. B. Kibble, G. Lazarides and Q. Shafi, *Strings in $SO(10)$* , *Phys. Lett. B* **113** (1982) 237–239.

[45] R. Jeannerot, *A Supersymmetric $SO(10)$ model with inflation and cosmic strings*, *Phys. Rev. D* **53** (1996) 5426–5436, [[hep-ph/9509365](#)].

[46] M. Kawasaki, K. Kohri, T. Moroi and Y. Takaesu, *Revisiting Big-Bang Nucleosynthesis Constraints on Long-Lived Decaying Particles*, *Phys. Rev. D* **97** (2018) 023502, [[1709.01211](#)].

[47] V. Berezinsky and O. Kalashev, *High energy electromagnetic cascades in extragalactic space: physics and features*, *Phys. Rev. D* **94** (2016) 023007, [[1603.03989](#)].

[48] M. Hindmarsh, J. Lizarraga, J. Urrestilla, D. Daverio and M. Kunz, *Scaling from gauge and scalar radiation in Abelian Higgs string networks*, *Phys. Rev. D* **96** (2017) 023525, [[1703.06696](#)].

[49] J. J. Blanco-Pillado, K. D. Olum and B. Shlaer, *The number of cosmic string loops*, *Phys. Rev. D* **89** (2014) 023512, [[1309.6637](#)].

[50] J. J. Blanco-Pillado and K. D. Olum, *Stochastic gravitational wave background from smoothed cosmic string loops*, *Phys. Rev. D* **96** (2017) 104046, [[1709.02693](#)].

[51] L. Lorenz, C. Ringeval and M. Sakellariadou, *Cosmic string loop distribution on all length scales and at any redshift*, *JCAP* **10** (2010) 003, [[1006.0931](#)].

[52] C. Ringeval, M. Sakellariadou and F. Bouchet, *Cosmological evolution of cosmic string loops*, *JCAP* **02** (2007) 023, [[astro-ph/0511646](#)].

[53] K. D. Olum and J. J. Blanco-Pillado, *Field theory simulation of Abelian Higgs cosmic string cusps*, *Phys. Rev. D* **60** (1999) 023503, [[gr-qc/9812040](#)].

[54] P. Auclair, D. A. Steer and T. Vachaspati, *Particle emission and gravitational radiation from cosmic strings: observational constraints*, *Phys. Rev. D* **101** (2020) 083511, [[1911.12066](#)].

[55] P. Auclair, K. Leyde and D. A. Steer, *A window for cosmic strings*, [2112.11093](#).

[56] Y. Gouttenoire, G. Servant and P. Simakachorn, *Beyond the Standard Models with Cosmic Strings*, *JCAP* **07** (2020) 032, [[1912.02569](#)].

[57] PLANCK collaboration, N. Aghanim et al., *Planck 2018 results. VI. Cosmological parameters*, *Astron. Astrophys.* **641** (2020) A6, [[1807.06209](#)].

[58] G. Bélanger, F. Boudjema, A. Goudelis, A. Pukhov and B. Zaldivar, *micrOMEGAs5.0 : Freeze-in*, *Comput. Phys. Commun.* **231** (2018) 173–186, [[1801.03509](#)].

[59] P. Gondolo and G. Gelmini, *Cosmic abundances of stable particles: Improved analysis*, *Nucl. Phys. B* **360** (1991) 145–179.

[60] M. Yamada and K. Yonekura, *Cosmic strings from pure Yang-Mills theory*, [2204.13123](#).

[61] PLANCK collaboration, P. A. R. Ade et al., *Planck 2015 results. XIII. Cosmological parameters*, *Astron. Astrophys.* **594** (2016) A13, [[1502.01589](#)].

[62] J. Lizarraga, J. Urrestilla, D. Daverio, M. Hindmarsh and M. Kunz, *New CMB constraints for Abelian Higgs cosmic strings*, *JCAP* **10** (2016) 042, [[1609.03386](#)].

[63] FERMI-LAT collaboration, M. Ackermann et al., *The spectrum of isotropic diffuse gamma-ray emission between 100 MeV and 820 GeV*, *Astrophys. J.* **799** (2015) 86, [[1410.3696](#)].

[64] P. Bhattacharjee and G. Sigl, *Origin and propagation of extremely high-energy cosmic rays*, *Phys. Rept.* **327** (2000) 109–247, [[astro-ph/9811011](#)].

[65] C. Gowling, M. Hindmarsh, D. C. Hooper and J. Torrado, *Reconstructing physical parameters from template gravitational wave spectra at LISA: first order phase transitions*, [2209.13551](#).

[66] J. Hazboun, J. Romano and T. Smith, *Hasasia: A python package for pulsar timing array sensitivity curves*, *Journal of Open Source Software* **4** (10, 2019) 1775.

[67] J. Hazboun, “Pulsar Timing Array GW Astronomy Update.”
URL: https://dcc.ligo.org/public/0177/G2101389/001/jsh_gwanw_2021.pdf, 2021.

[68] K. Griest and M. Kamionkowski, *Unitarity Limits on the Mass and Radius of Dark Matter Particles*, *Phys. Rev. Lett.* **64** (1990) 615.

- [69] FERMI-LAT collaboration, M. Ackermann et al., *Constraining Dark Matter Models from a Combined Analysis of Milky Way Satellites with the Fermi Large Area Telescope*, *Phys. Rev. Lett.* **107** (2011) 241302, [[1108.3546](#)].
- [70] N. Sahu, P. Bhattacharjee and U. A. Yajnik, *B - L cosmic strings and baryogenesis*, *Phys. Rev. D* **70** (2004) 083534, [[hep-ph/0406054](#)].
- [71] W. Buchmüller, V. Domcke, K. Kamada and K. Schmitz, *The Gravitational Wave Spectrum from Cosmological B - L Breaking*, *JCAP* **10** (2013) 003, [[1305.3392](#)].
- [72] W. Buchmuller, V. Domcke, H. Murayama and K. Schmitz, *Probing the scale of grand unification with gravitational waves*, *Phys. Lett. B* **809** (2020) 135764, [[1912.03695](#)].